should provide a useful alternate tool for the study of many active and passive systems which have been studied using the coupled-mode theory.

REFERENCES

[1] G. I. Zysman and A. K. Johnson, "Coupled transmission line networks in an inhomogeneous dielectric medium," *IEEE Trans. Microwave Theory Tech.*, vol. MTT-17, pp. 753–759, Oct. 1969.

[2] E. M. T. Jones and J. T. Bolljahn, "Coupled-strip-transmission-line filters and directional couplers," *IRE Trans. Microwave Theory Tech.*, vol. MTT-4, pp. 75–81, Apr. 1956.

[3] H. Ozaki and J. Ishii, "Synthesis of a class of strip-line filters," *IRE Trans. Circuit Theory*, vol. CT-5, pp. 104–109, June 1958.

[4] E. G. Vlostovskiy, "Theory of coupled transmission lines," *Telecommun. Radio Eng.*, vol. 21, pp. 87–93, Apr. 1967.

[5] R. A. Speciale, "Fundamental even- and odd-mode waves for nonsymmetrical coupled lines in non-homogeneous media," in *1974 IEEE MTT Int. Microwave Symp. Digest Tech. Papers*, June 1974, pp. 156–158.

[6] E. G. Cristal, "Coupled-transmission-line directional couplers with coupled lines of unequal characteristic impedance," *IEEE Trans. Microwave Theory Tech.*, vol. MTT-14, pp. 337–346, July 1966.

[7] C. B. Sharpe, "An equivalence principle for nonuniform transmission line directional couplers," *IEEE Trans. Microwave Theory Tech.*, vol. MTT-15, pp. 398–405, July 1967.

[8] H. Amemiya, "Time domain analysis of multiple parallel transmission lines," *RCA Rev.*, vol. 28, pp. 241–276, June 1967.

[9] M. K. Krage and G. I. Haddad, "Characteristics of coupled microstrip transmission lines—I: Coupled-mode formulation of inhomogeneous lines," *IEEE Trans. Microwave Theory Tech.*, vol. MTT-18, pp. 217–222, Apr. 1970.

[10] K. D. Marx, "Propagation modes, equivalent circuits, and characteristic terminations for multiconductor transmission lines with inhomogeneous dielectrics," *IEEE Trans. Microwave Theory Tech.*, vol. MTT-21, pp. 450–457, July 1973.

[11] B. M. Oliver, "Directional electromagnetic couplers," *Proc. IRE*, vol. 42, pp. 1686–1692, Nov. 1954.

Long-Wavelength Electromagnetic Power Absorption in Prolate Spheroidal Models of Man and Animals

CURTIS C. JOHNSON, SENIOR MEMBER, IEEE, CARL H. DURNEY, MEMBER, IEEE, AND HABIB MASSOUDI, STUDENT MEMBER, IEEE

Abstract—**A previously developed electromagnetic (EM) field perturbation analysis is used to calculate the electric fields in tissue prolate spheroids irradiated by plane waves with long wavelength compared to the spheroid dimensions. This theory is applied to prolate spheroid models of man and animals to obtain internal electric field strength, absorbed power distribution, and total absorbed power. These data are of value in estimating tissue EM power absorption in experimental animals and man. The theory may be used to help extrapolate animal biological effects data to man, and as a guide to establishing an EM radiation safety standard.**

INTRODUCTION

An important aspect of electromagnetic- (EM) wave biological-effects research involves the investigation of internal electric field strength and power absorption in biological tissue subjected to EM irradiation. EM power is absorbed by the tissues as a function of frequency, body shape, tissue properties, and irradiation conditions. Absorbed power increases as the square of frequency at long wavelengths, enters a transition region of maximum absorbed power when the wavelength approximates body dimensions, and then decreases with frequency due to skin-effect surface heating. This general behavior has been characterized by Johnson and Guy [1] for a tissue sphere model, and has been measured experimentally by Gandhi [2] in irradiation experiments with rats.

Early work on the tissue sphere model has been done by Anne *et al.* [3], Shapiro *et al.* [4], Kritikos and Schwan [5], and Johnson and Guy [1]. Recent analyses of multilayer effects in spherical models have been reported by Joines and Spiegel [6], and Weil [7]. The principal result of the multilayer model compared to the homogeneous model is a shift in resonant frequency and an increase of peak absorption. These theoretical approaches are applicable to all frequency ranges and require extensive computer computations. Simpler low-frequency Mie solutions have been obtained by Lin *et al.* [8].

A field perturbation approach has recently been developed and applied to prolate spheroid models for low ka values well below the maximum absorption frequency range [9]. A principal conclusion from the prolate spheroid results is that orientation of the body with respect to the incident plane-wave vectors is an extremely important variable which can make an order-of-magnitude difference in EM power absorption.

Considerable effort has also been expended to measure

Manuscript received October 9, 1974; revised April 14, 1975. This work was supported by the USAF School of Aerospace Medicine, Brooks Air Force Base, Tex. 78235.

C. C. Johnson is with the Department of Bioengineering, University of Utah, Salt Lake City, Utah 84112.

C. H. Durney is with the Department of Electrical Engineering and the Department of Bioengineering, University of Utah, Salt Lake City, Utah 84112.

H. Massoudi is with the Department of Electrical Engineering, University of Utah, Salt Lake City, Utah 84112.

absorbed power and energy in real animals. This includes work by Justesen [10], [11], Ho's development of a 2450-MHz-waveguide irradiation facility [12], and whole-body calorimetry [13]. Guy and Korbel [14] have evaluated absorbed power in a cavity animal irradiation system. Gandhi [2] has used transmitted and reflected power measurements in a stripline irradiation chamber to measure absorbed power in mice and rats. Similar tests in a large-scale facility are under way by Frazer and Allen [15]. Considerable insight and quantitative information has been obtained by Guy using bisected killed animals and animal phantoms with thermographic camera measurements [1].

The major objective of this paper is to determine the time-averaged volumetric tissue-absorbed power density, defined as the time rate at which energy is absorbed by the tissue. Absorbed power density in watts per unit volume is the time rate of absorbed energy density in joules per unit volume. One watt is defined as 1 J/s. Absorbed power density is often called power dissipation. For example, if a homogeneous resistor of 5 volume units uniformly dissipates 10 W, we say the absorbed power density in the resistor material is 2 W/unit volume. Volumetric tissue-absorbed power density or power dissipation is not to be confused with surface-transmitted electromagnetic power density or Poynting's vector with units of watts per square meter. The time-averaged Poynting's vector is defined as $\bar{\boldsymbol{P}} = \frac{1}{2}$ Re $\boldsymbol{E} \times \boldsymbol{H}^*$ watts per square meter where * denotes complex conjugate. The time-averaged volumetric tissue-absorbed power density is $\bar{\mathcal{P}}_L = \frac{1}{2}\sigma \boldsymbol{E} \cdot \boldsymbol{E}^*$ W/m^3, where σ is the tissue conductivity. When a tissue body of volume V in an enclosing surface S is irradiated, the closed-surface integral of $\bar{\boldsymbol{P}}$ over S is, by energy conservation principles, equal to the volume integral of $\bar{\mathcal{P}}_L$ over the enclosed tissue volume V. In this paper we use the concept of rate of absorbed energy density or dose rate (absorbed power density) common in EM field theory, rather than the concept of dose (absorbed energy density) common in ionizing radiation. By implication we infer that absorbed power density is the important parameter for hazard assessment, rather than absorbed energy or dose.

In this paper the low ka perturbation theory is applied to prolate spheroid models of man and experimental animals to obtain internal EM absorbed power distributions and total absorbed power for different orientations and frequencies. Some preliminary experimental data obtained by others are cited to confirm the theoretical absorbed power calculations.

THEORETICAL BASIS

The perturbation theory used in the calculations [9] is based on the method outlined by Van Bladel [16]. A prolate spheroid tissue body is isolated in free space and illuminated by a linearly polarized EM plane wave. The incident, scattered, and tissue fields are expanded in a power series in $(-jk)$, where $j = (-1)^{1/2}$, and k is the free-space propagation constant. The field boundary conditions are written in prolate spheroidal coordinates, and the first-order field terms obtained. The prolate spheroid has a major axis a, a minor axis b, and is assumed to be composed of material with dielectric constant and conductivity equal to that of muscle tissue. The tissue complex-dielectric-constant values used in the analysis are shown in Fig. 1 as a function of frequency, compiled from data published by Schwan [17] and Johnson and Guy [1].

Once the tissue electric fields are obtained, the time-averaged absorbed EM power density is calculated from the equation

$$\bar{\mathcal{P}}_L = \tfrac{1}{2}\sigma \boldsymbol{E} \cdot \boldsymbol{E}^*. \tag{1}$$

In this paper we will express $\bar{\mathcal{P}}_L$ in units of watts per kilogram of tissue mass, assuming tissue density of 1 g/cm^3. The total time-averaged power absorbed by the spheroid is given by the volume integral of (1) over the prolate spheroid. Three specific solutions are carried out, one for each of the three possible orientations of the prolate spheroid major axis with respect to the field vectors in the linearly polarized planewave. These three cases are denoted as magnetic polarization when the magnetic vector is aligned with the spheroid long axis (subscript h), electric polarization when the electric vector is aligned with the spheroid axis (subscript e), and cross polarization when the spheroid axis is perpendicular to both the electric and magnetic vectors in the plane wave (subscript c). The EM absorbed power density in the tissue for these three cases, respectively, are [9]

$$\bar{\mathcal{P}}_{Lh} = \tfrac{1}{2}\sigma k^2[(B_h/\sigma\eta_0)^2 - (B_h/\sigma\eta_0) r \sin\phi + r^2/4] \tag{2}$$

$$\bar{\mathcal{P}}_{Le} = \tfrac{1}{2}\sigma k^2[(B_e/\sigma\eta_0)^2 - 2B_e a^2 r \sin\phi/\sigma\eta_0\,(a^2+b^2) + a^4 r^2 \sin^2\phi/(a^2+b^2)^2 + b^4 z^2/(a^2+b^2)^2] \tag{3}$$

$$\bar{\mathcal{P}}_{Lc} = \tfrac{1}{2}\sigma k^2[(B_h/\sigma\eta_0)^2 - 2B_h b^2 z/\sigma\eta_0(a^2+b^2) + b^4 z^2/(a^2+b^2)^2 + a^4 r^2 \cos^2\phi/(a^2+b^2)^2] \tag{4}$$

where the expressions have been written in cylindrical coordinates, and where

$$\eta_0 = (\mu_0/\epsilon_0)^{1/2};$$

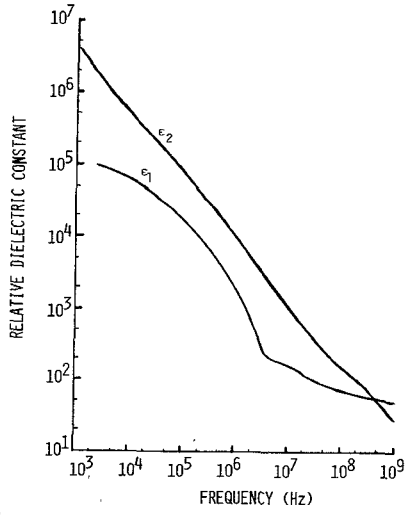

Fig. 1. The real part ϵ_1 and the imaginary part ϵ_2 of the relative dielectric constant for high water-content tissue. This plot is compiled from data published by Schwan and Guy.

k $= \omega(\mu_0\epsilon_0)^{1/2}$;
σ frequency-dependent tissue conductivity;
$2a$ length of prolate spheroid major axis;
$2b$ width of prolate spheroid minor axis;
$B_h = 2[u_{10}^2 - 1]^{-1}[u_{10}^2/(u_{10}^2 - 1) - (\frac{1}{2})u_{10} \ln [(u_{10} + 1)/(u_{10} + 1)]]^{-1}$;
$B_e = [u_{10}^2 - 1]^{-1}[(u_{10}/2) \ln \cdot[(u_{10} + 1)/(u_{10} - 1)] - 1]^{-1}$;
$u_{10} = a/(a^2 - b^2)^{1/2}$.

Integration over the volume of the prolate spheroid gives the total time-averaged absorbed EM power density

$$\bar{P}_{Lh} = \tfrac{1}{2}\sigma k^2 V[(B_h/\sigma\eta_0)^2 + b^2/10] \quad (5)$$

$$\bar{P}_{Le} = \tfrac{1}{2}\sigma k^2 V[(B_e/\sigma\eta_0)^2 + a^2b^2/5(a^2 + b^2)] \quad (6)$$

$$\bar{P}_{Lc} = \tfrac{1}{2}\sigma k^2 V[(B_h/\sigma\eta_0)^2 + a^2b^2/5(a^2 + b^2)] \quad (7)$$

where V is the spheroidal volume $V = 4\pi ab^2/3$. These equations reduce to the corresponding sphere equations of Lin *et al.* [8], for $b \to a$. These equations are valid when the object dimensions a and b are long compared to a wavelength. The ka limit of validity has not been firmly established. Preliminary investigations of the second terms in the field expansion indicate that (5)–(7) are valid for a man-size spheroid with $a = 0.875$ m, and $b = 0.138$ m, up to about 30 MHz.

In the above equations the z axis is always aligned with the long axis of the spheroid. For magnetic polarization the plane-wave E-vector is aligned with the x axis; the H-vector is aligned with the z axis. For electric polarization, the plane-wave E-vector is aligned with the z-axis; the H-vector is aligned with the x axis. For cross polarization the plane-wave E-vector is aligned with the $-x$ axis; the H-vector is aligned with the y axis.

INTERNAL POWER ABSORPTION

In order to obtain a quantitative description of the absorbed EM power distribution within the prolate spheroid, (2)–(4) are used to calculate $\bar{P}_L$ along the x, y, and z axes. We first consider a 70-kg prolate spheroid of high water-content tissue, with major-to-minor axis ratio $a/b = 1.5$. In this case we do not deviate significantly from the sphere configuration; thus the results should resemble the power absorption patterns obtained from the spherical Mie solution of Lin *et al.* [8]. Solutions have been carried out at several frequencies below 30 MHz, and the results are quantitatively similar. Data for 10 MHz are shown in Figs. 2–4 to illustrate the results.

Fig. 2 shows the relative absorbed power density along the three axes for magnetic polarization. The plots are very similar to the sphere results. The power absorption is caused by an internal electric polarization field along the x axis induced by the plane-wave E-field, combined with a circulating electric field pattern around the z axis. The currents produced by this magnetically induced circulating E-field are the familiar eddy currents induced by the incident H-field. These eddy currents are zero on the z axis; thus a low relative absorbed power density is seen along the z axis, resulting only from the electric polarization field. A parabolic absorbed power density pattern along the x axis is observed, resulting from a superposition of the electric polarization fields and the eddy-current fields. Along the y axis, the two induced field components add asymetrically to generate a displaced parabolic power density pattern, with peak heating on the surface of the prolate spheroid which first intercepts the plane wave.

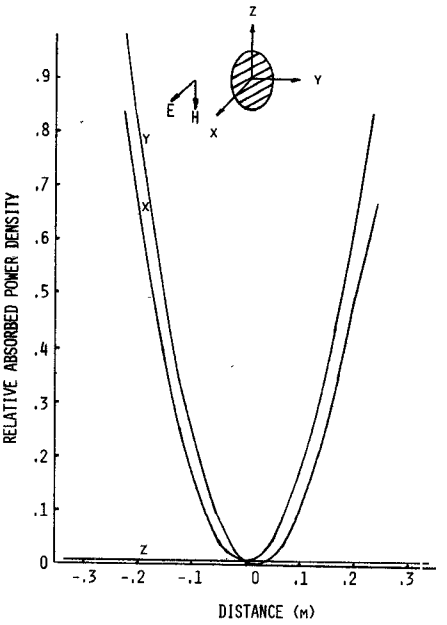

Fig. 2. Relative absorbed power density along the x, y, and z axes of a prolate spheroid, magnetic polarization. $a/b = 1.5$, $a = 0.335$ m, $f = 10$ MHz, volume = 0.07 m³. The maximum absorbed power density is 1.59×10^{-3} W/kg for a 1-mW/cm² incident power density.

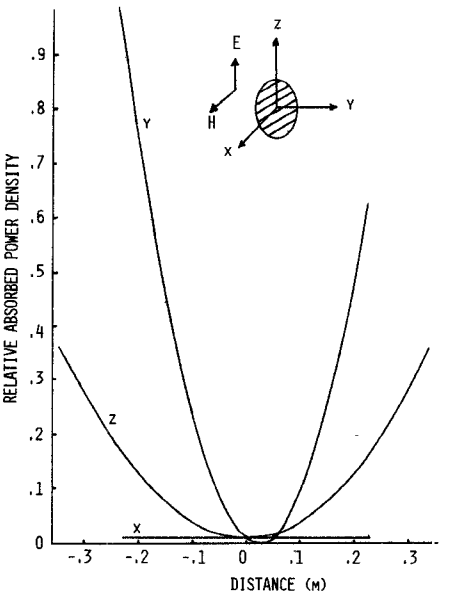

Fig. 3. Relative absorbed power density along the x, y, and z axes of a prolate spheroid, electric polarization. $a/b = 1.5$, $a = 0.335$ m, $f = 10$ MHz, volume = 0.07 m³. The maximum power density is 3.14×10^{-3} W/kg for a 1-mW/cm² incident power density.

For the case of electric polarization, as shown in Fig. 3, the electric polarization fields are along the z axis and the eddy-current fields circulate around the x axis. Since the eddy-current fields are zero along the x axis, a low relative

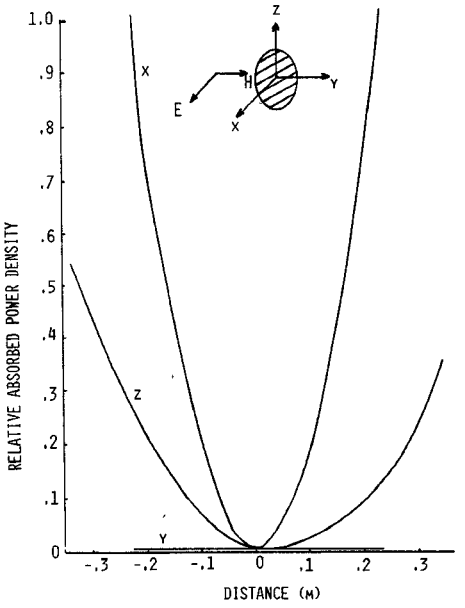

Fig. 4. Relative absorbed power density along the x, y, and z axes of a prolate spheroid, cross polarization. $a/b = 1.5$, $a = 0.335$ m, $f = 10$ MHz, volume = 0.07 m^3. The maximum absorbed power density is 2.54×10^{-3} W/kg for a 1-mW/cm^2 incident power density.

absorbed power density is generated along the x axis by the polarization fields alone. Parabolic absorbed power density patterns are again observed along the y and z axes, with greatly enhanced absorbed power along the y axis. The peak absorbed power density in this case is 3.14×10^{-3} W/kg for a 1-mW/cm^2 incident plane-wave power density, compared to only 1.59×10^{-3} W/kg for the magnetic polarization case. The higher absorbed power density can be attributed to two factors. One is greater total eddy-current flow resulting from the spheroid intercepting a much larger total magnetic flux in this orientation. The eddy currents circulate in the yz plane, concentrating as they cross the y axis because the path width narrows, and weakening as they cross the z axis because the path width broadens. This causes higher fields generating a higher peak absorbed power density along the y axis. The other factor contributing to the higher absorbed power density is that the internal electric field induced by the incident electric field is stronger. This occurs because the field boundary conditions require the tangential electric field to be continuous, and since the spheroid in this orientation has more surface parallel to the incident electric field, the internal field is more nearly equal to the incident field. Thus both the magnetically induced and electrically induced internal electric fields are stronger for electric polarization than for magnetic polarization.

Power density patterns for cross polarization are illustrated in Fig. 4. In this case the electric vector generates electric polarization fields along the x axis, and the magnetic field induces eddy-current electric fields circulating around the y axis. Again, strong magnetically induced internal electric fields are present, due to the greater magnetic flux intercepted by the prolate spheroid body. This causes an intense parabolic heating pattern along the x axis. Since no eddy-current fields exist along the y axis, a low relative absorbed power density is observed there. The two induced internal field components combine to generate a displaced parabolic pattern along the z axis. Whereas in both the electric and magnetic polarization cases the maximum absorbed power density occurs at the surface of the prolate spheroid first intercepted by the plane wave, this is not the case for cross polarization. Maximum absorbed power density occurs at $x = \pm b$, where the eddy-current fields are most concentrated. Note also in this case that the peak internal absorbed power density is somewhat lower than in the electric polarization case but still higher than for magnetic polarization. This occurs because the magnetically induced internal electric field is strong as in the case of electric polarization, but the electrically induced internal electric field is weaker than for electric polarization. It is weaker because the boundary conditions on the normal fields require the ratio of the external and internal fields to be equal to the dielectric constant and consequently the internal field is weaker. Since the spheroid long axis is normal to the incident electric field in this polarization, the internal field is thus weaker than for electric polarization. It might be said that the spheroid is "shielded" from the incident electric field in both the cross and magnetic polarizations.

We now consider a more elongated prolate spheroid with $a/b = 6.34$, $a = 0.875$ m, and volume = 0.07 m^3, which closely corresponds to the man model. Fig. 5 gives the results for magnetic polarization, showing the same qualitative results as in Fig. 2. Note that the thinning of the prolate spheroid has reduced the intercepted magnetic flux, causing lower eddy currents, and thus a lower maximum absorbed power. Fig. 6 shows the striking result for electric polarization, where the internal power patterns are considerably different than the corresponding case of Fig. 3. Note that the maximum absorbed power density is approximately twice as high as in Fig. 3. The absorbed power density along the x axis is elevated considerably, indicative of much stronger coupling of the external electric field into the interior of the prolate spheroid. The longer spheroid has forced the internal electric field to more closely correspond to the incident field because of the

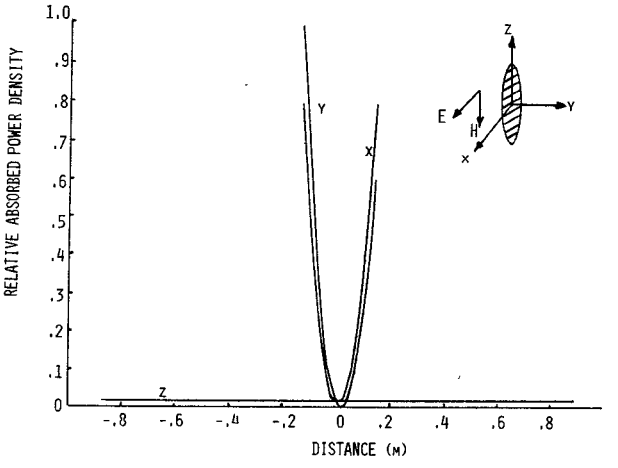

Fig. 5. Relative absorbed power density along the x, y, and z axes of a prolate spheroid, magnetic polarization. $a/b = 6.34$, $a = 0.875$ m, $f = 10$ MHz, volume = 0.07 m^3. The maximum absorbed power density is 6.38×10^{-4} W/kg for a 1-mW/cm^2 incident power density.

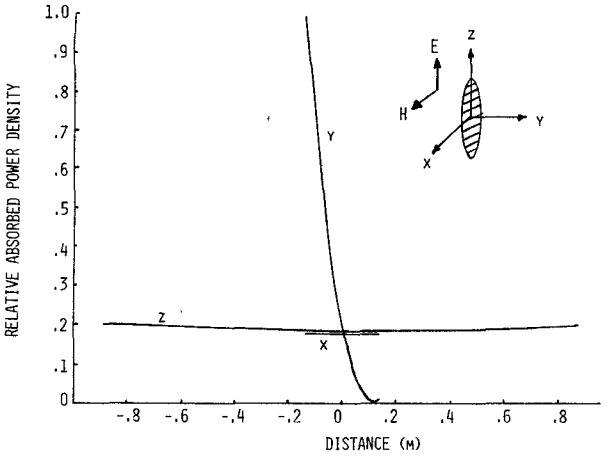

Fig. 6. Relative absorbed power density along the x, y, and z axes of a prolate spheroid, electric polarization. a/b = 6.34, a = 0.875 m, f = 10 MHz, volume = 0.07 m³. The maximum absorbed power density is 6.14 × 10^{-3} W/kg for a 1-mW/cm² incident power density.

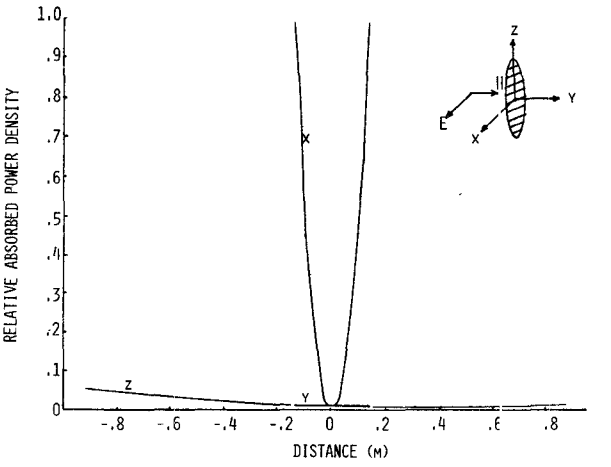

Fig. 7. Relative absorbed power density along the x, y, and z axes of a prolate spheroid, cross polarization. a/b = 6.34, a = 0.875 m, f = 10 MHz, volume = 0.07 m³. The maximum absorbed power density is 1.93 × 10^{-3} W/kg for a 1-mW/cm² incident power density.

boundary condition for tangential electric fields. The relatively flat power distribution along the z axis indicates a strong electric polarization field, with relatively weak eddy-current fields because of the smaller intercepted magnetic flux. Distribution along the y axis is totally different, indicating a predominant electric-field-induced internal power absorption, with peak power absorption on the surface of the prolate spheroid first struck by the incident plane wave. For cross polarization, where again the electric field is along the minor axis of the spheroid, the spheroid is shielded from the plane-wave electric field. Fig. 7 shows the expected result with peak absorbed power density along the x axis. Clearly eddy-current-field-induced power absorption predominates. Note in these cases there is approximately an order-of-magnitude difference in the peak absorbed power density in the spheroid, depending on orientation of the spheroid with respect to the plane-wave field vectors.

ABSORBED ELECTROMAGNETIC POWER IN ANIMAL MODELS

This section presents quantitative data on the average and peak absorbed power density in models of a variety of biological animals. Using this data, experimenters will be able to estimate the internal power absorption for each animal, knowing the incident plane-wave intensity. Biological effects data may then be correlated with internal absorbed power density information.

The average weight, height, and resulting a/b ratio for man and several useful experimental animals are given in Table I. These data are used in the calculations which follow.

Although it has not been firmly established what limiting value of ka is allowed in the theory, preliminary experimental correlations indicate the theory is valid up to 30 MHz for the man-sized spheroid. A comparison between the first-order solution and the exact Mie solution for the sphere has been made by Lin [8], who has established a reasonable correlation out to approximately 25 MHz.

Using data for the average man, the average and peak absorbed power density for the three orientations is shown in Fig. 8 for a 1-mW/cm² incident plane-wave power density. Note the absorbed power density increases as approximately the square of frequency, and there is a strong orientational effect with the electric polarization inducing approximately one order of magnitude greater absorbed power density than the magnetic polarization. Cross polarization is intermediate. Fig. 9 illustrates the corresponding data for the dog, with the frequency range extended out to 50 MHz due to lower ka values, assuming a constant limiting ka constraint on the validity of this first-order theory. Corresponding data for the monkey are shown in Fig. 10, the rabbit in Fig. 11, the rat in Fig. 12, and the mouse in Fig. 13. In each case the frequency range is extended under the constant limiting ka constraint.

A typical irradiation condition is shown in Fig. 14, where a microwave horn generates a near plane wave in the far field which irradiates a 20-g mouse. A field survey meter may be used to establish the plane-wave power density at the position of the mouse. For example, assume the field meter at the position of the mouse reads 150 mW/cm². In this configuration the magnetic field vector is aligned with the long axis of the mouse; thus we have

TABLE I

Species	Average Weight (Kg)	Average Height, 2a (m)	a/b
Man	70.0	1.75	6.34
Dog	15.0	1.12	7.0
Monkey	3.0	0.66	7.0
Rabbit	1.0	0.40	5.8
Rat	0.20	0.15	3.0
Mouse	0.02	0.0536	2.0

Note: Biological data for several species, and the calculated a/b ratio for the prolate spheroid model, taken from *Collier's Encyclopedia*, vol. 19, and *Encyclopedia Britannica*, vol. 7.

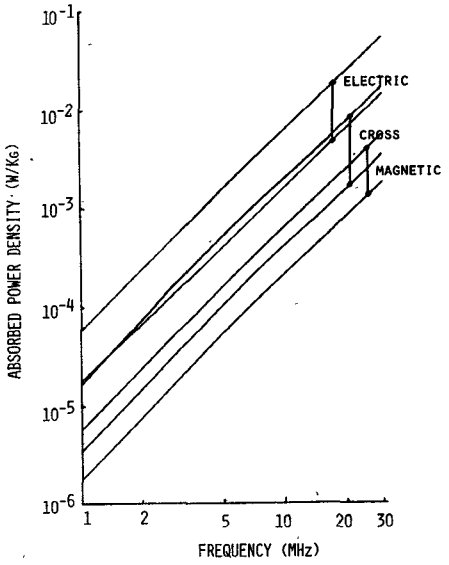

Fig. 8. Average and peak absorbed power density in a prolate spheroid model of man, for the three possible polarizations. a/b = 6.34, a = 0.875 m, volume = 0.07 m³. Incident power density is 1 mW/cm².

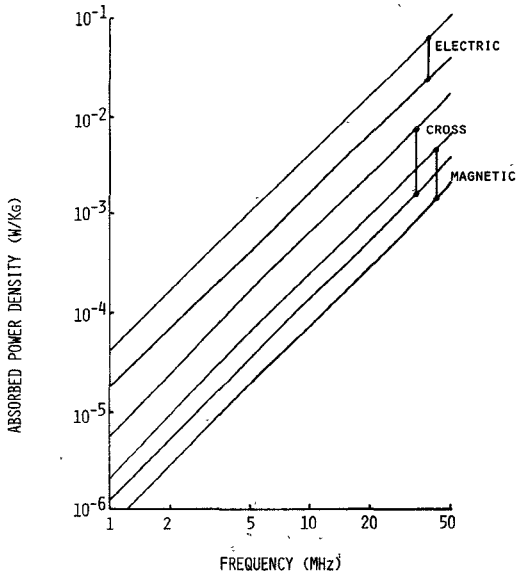

Fig. 9. Average and peak absorbed power density in a prolate spheroid model of the dog, for the three possible polarizations. a/b = 7.0, a = 0.56 m, volume = 0.015 m³. Incident power density is 1 mW/cm².

magnetic polarization. At 915 MHz the peak and average absorbed power density in the mouse may be obtained from Fig. 13 with approximate values of 0.064 W/kg average, and 0.22 W/kg peak for 1-mW/cm² incident intensity. The localized peak absorbed power density is on the side of the mouse facing the horn, and the mouse is subjected to considerable eddy currents circling his body. Since the incident power density is 150 mW/cm², the peak absorbed power density is 33 W/kg, assuming a density of 1 g/cm³. The average absorbed power density is 9.6 W/kg, and the total absorbed power is 0.192 W.

The information given in Figs. 8–13 may also be very useful in extrapolating tissue-absorbed power in animal experiments to expected tissue-absorbed power in man

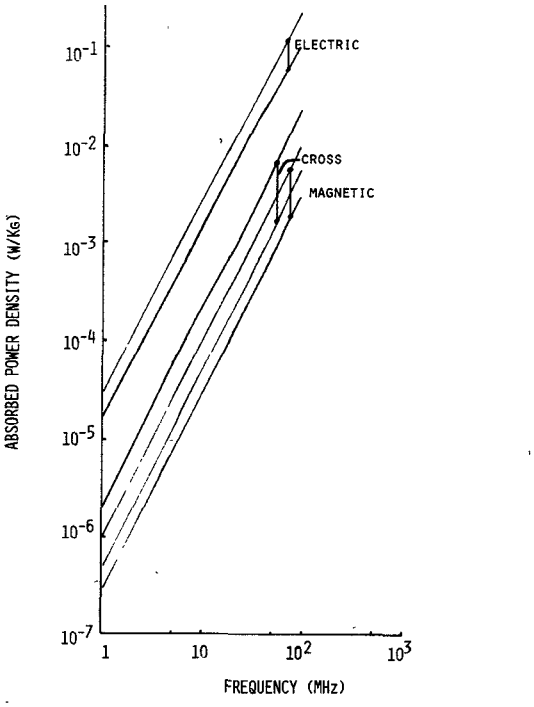

Fig. 10. Average and peak absorbed power density in a prolate spheroid model of the monkey, for the three possible polarizations. a/b = 7.0, a = 0.33 m, volume = 0.003 m³. Incident power density is 1 mW/cm².

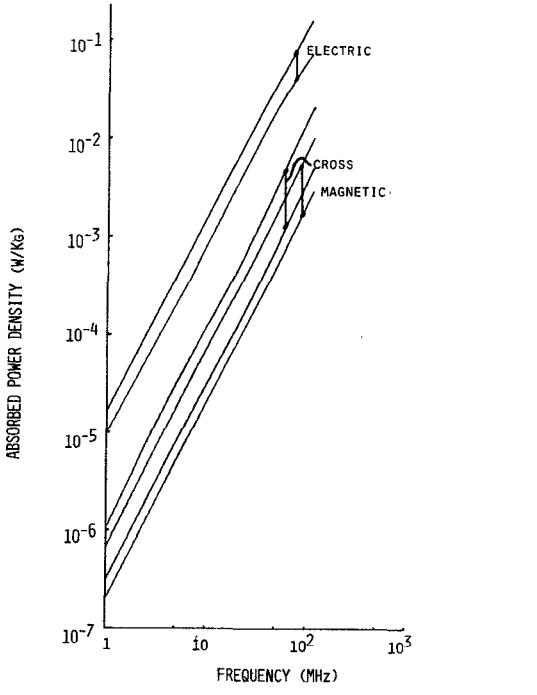

Fig. 11. Average and peak absorbed power density in a prolate spheroid model of the rabbit, for the three possible polarizations. a/b = 5.8, a = 0.2 m, volume = 0.001 m³. Incident power density is 1 mW/cm².

under similar irradiation conditions. For example, suppose a biological effect is discovered in a mouse irradiated at an incident power density of 10 W/cm² with electric polarization at a frequency of 20 MHz. From Fig. 13, the average absorbed power density for this case is approximately 2.5 W/kg. If the biological effect were related to average absorbed power density, one might expect to see a similar

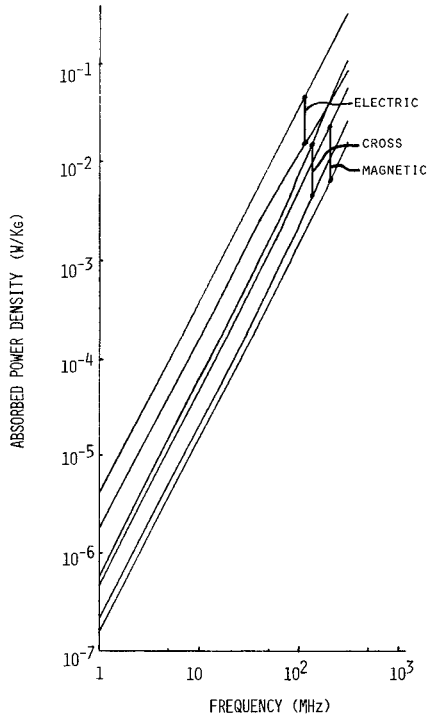

Fig. 12. Average and peak absorbed power density in a prolate spheroid model of the rat, for the three possible polarizations. a/b = 3.0, a = 0.075 m, volume = 0.0002 m³. Incident power density is 1 mW/cm².

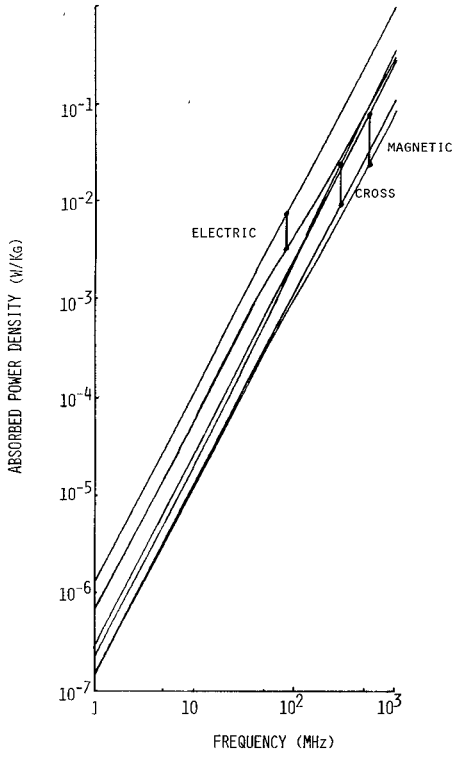

Fig. 13. Average and peak absorbed power density in a prolate spheroid model of the mouse, for the three possible polarizations. a/b = 2.0, a = 0.0268 m, volume = 0.00002 m³. Incident power density is 1 mW/cm².

effect in man at about the same average absorbed power density, and without the information given in Figs. 8 and 13, one might at first conclude that the same effect would be seen in man irradiated with the same incident power

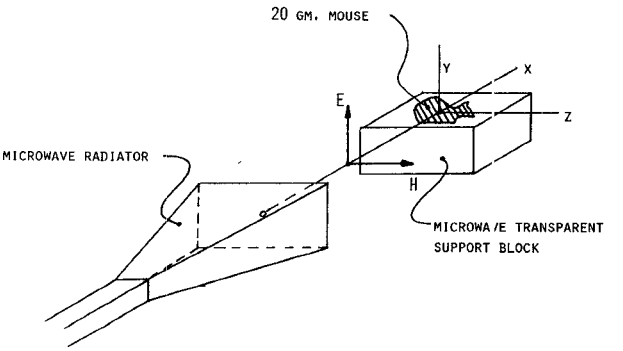

Fig. 14. Typical microwave irradiation configuration showing a mouse subjected to plane-wave radiation under magnetic polarization.

density. However, from Fig. 8, it can be seen that at 20 MHz the average absorbed power density in man irradiated by 10 W/cm² with electric polarization is approximately 67 W/kg, which is nearly 27 times greater than that of the mouse. Thus the same average tissue-absorbed power is expected in man at an incident power density of approximately 370 mW/cm² as that in the mouse at an incident power density of 10 W/cm².

When an animal is irradiated under conditions to which neither of the three orthogonal polarizations apply, then the original equations for absorbed power density must be rederived in terms of the electric field components present. It has been demonstrated for two specific cases that in the case of arbitrary polarization, the plane wave may be reduced to its two component polarizations, and the power contributions allocated according to (5)–(7). For example, Fig. 15 shows the effect of polarization with the electric vector at an angle θ from the z axis, H always along the x axis. In this case, ranging from $\theta = 0°$ to 90° corresponds to ranging from electric to cross polarization. Fig. 16 shows the comparable calculations ranging from electric polarization to magnetic polarization.

INCIDENT PLANE-WAVE POWER DENSITY CHANGES FOR CONSTANT TISSUE-ABSORBED POWER

The incident plane-wave power density must be greatly increased, as frequency is reduced, in order to produce the same fields and absorbed power density in the tissues. Since it is suspected that biological effects of RF radiation are caused by the presence of electric field and power density in the tissues and organs, a knowledge of incident power density variation corresponding to constant tissue fields as a function of frequency may be valuable in future consideration of EM radiation safety standards. The incident plane-wave power density required to generate within the prolate spheroid the same peak or average absorbed power density as that present at 10 MHz with an incident power density of 1 mW/cm² is plotted in Fig. 17. A frequency of 10 MHz is chosen as a reference point, since this corresponds to the lowest frequency in the present RF radiation protection standard. The worst case of electric polarization is depicted. Note the familar two-orders-of-

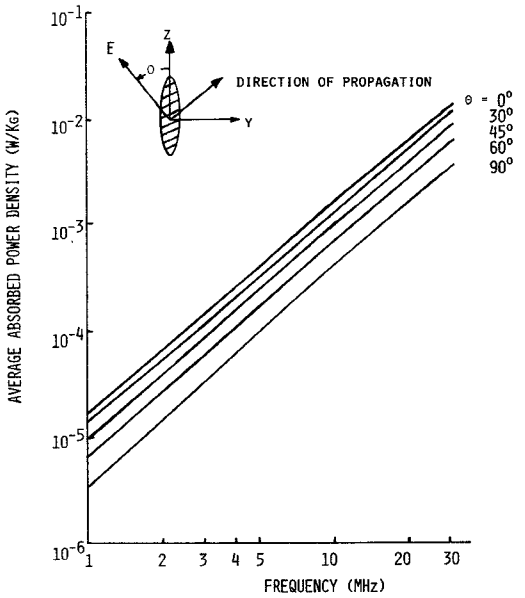

Fig. 15. Average absorbed power density in a prolate spheroid model of man, with polarizations intermediate between electric ($\theta = 0°$) and cross ($\theta = 90°$). $a/b = 6.34$, $a = 0.875$ m, volume = 0.07 m³. Incident power density is 1 mW/cm².

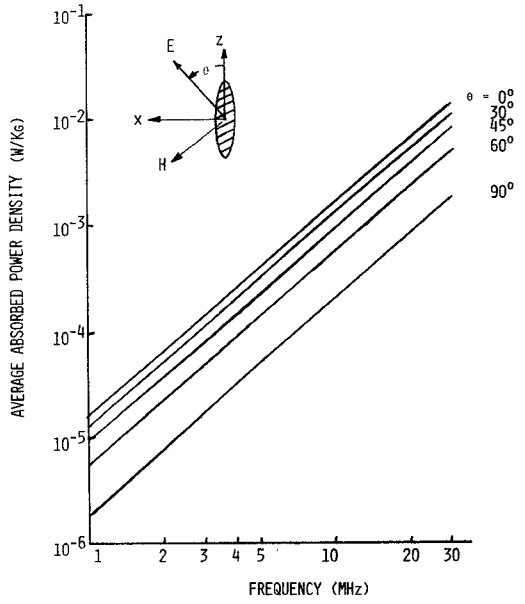

Fig. 16. Average absorbed power density in a prolate spheroid model of man, with polarization intermediate between electric ($\theta = 0°$) and magnetic ($\theta = 90°$). $a/b = 6.34$, $a = 0.875$ m, volume = 0.07 m³. Incident power density is 1 mW/cm².

magnitude increase in incident power density for one-order-of-magnitude decrease in frequency.

PRELIMINARY EXPERIMENTAL COMPARISONS

Several researchers have made experimental measurements of absorbed EM power density in animal models which may be used to evaluate these theoretical predictions. First, Gandhi [2] has made experimental measurements on prolate spheroids, rats and mice in a stripline exposure chamber. His tests were confined predominantly to the transition region of maximum power absorption and

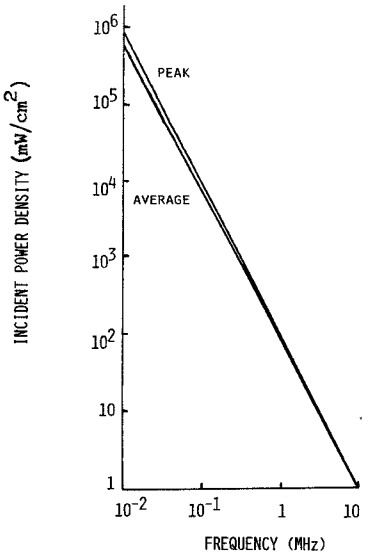

Fig. 17. Incident plane-wave power density required to produce the same average and peak absorbed power density in a prolate spheroid model of man as that produced at $f = 10$ MHz, 1 mW/cm², $a/b = 6.34$, $a = 0.875$ m, volume = 0.07 m³, electric polarization.

somewhat below, and thus do not provide a quantitative comparison. However, he observed substantially the same qualitative difference in power absorption as a function of orientation. Electric polarization produced by far the greatest power absorption, cross polarization being an intermediate case, and magnetic polarization produced the least power absorption.

Tests have been conducted by Allen [15] in a large-scale TEM transmission-line test chamber designed to operate in the 10–50-MHz range. The exposure chamber is 9.14 m long, 2.82 m wide, and 1.45 m high. A lucite human phantom was devised to approximate the dimensions of man, with base dimensions 45.7 cm by 78.8 cm. The phantom was filled with 90 kg of Ringer's solution, to a depth of 25 cm. Devising a best fit prolate spheroid for the human phantom, calculations were carried out to compare with the experimental results. Excellent agreement was obtained at 10 and 20 MHz, within the limits of experimental error, with some slight deviation at 30 MHz.

Guy [18] has conducted prolate spheroid phantom model irradiation tests in a 144-MHz resonant chamber. The phantom was located in a region of nearly pure electric field. After irradiation the phantom was split open and examined by means of a thermographic camera to estimate internal absorbed power density. This test was modeled theoretically by considering just the electrically induced polarization fields in the prolate spheroid model, and comparison calculations were made. A theoretical calculation of 5.19×10^{-6} W/kg peak absorbed power was obtained, compared to an experimental value of 6.15×10^{-6} W/kg.

Although these several preliminary indications indicate substantial agreement between experiment and theory, a systematic experimental examination of internal absorbed power is required to fully substantiate the theory and to establish the upper frequency limit of validity.

CONCLUSIONS

A field perturbation theory for prolate spheroid models of man and experimental animals has been used to obtain quantitative theoretical estimates of peak and average absorbed power and power distributions. There is a strong orientation effect which is obviously a critical factor in determining absorbed power. Theoretical data has been obtained for absorbed power distribution and total absorbed power for three orthogonal orientations of the prolate spheroid with respect to the plane-wave field vectors. These plots will be useful to biological researchers in obtaining tissue-absorbed-power-density estimates in terms of the incident plane-wave power density. Once biological effects due to tissue-absorbed power density are established, the plots may then be used to extrapolate back to find what incident plane-wave power densities generate the same tissue-absorbed power densities in the man model. This kind of extrapolation is essential for establishing a scientifically sound EM radiation safety standard.

REFERENCES

[1] C. C. Johnson and A. W. Guy, "Nonionizing electromagnetic wave effects in biological materials and systems," *Proc. IEEE*, vol. 60, pp. 692–718, June 1972.

[2] O. P. Gandhi, "A method of measuring RF absorption of whole animals and bodies of prolate spheroidal shapes," in *1974 Proc. Microwave Power Symp.* (Milwaukee, Wis.), May 28–31, 1974.

[3] A. Anne, M. Satio, O. M. Salati, and H. P. Schwan, "Relative microwave absorption cross section of biological significance," in *Biological Effects of Microwave Radiation*, vol. 1. New York: Plenum, 1960, pp. 153–176.

[4] A. R. Shapiro, R. F. Lutomirski, and H. T. Yura, "Induced fields and heating within a cranial structure irradiated by an electromagnetic plane wave," *IEEE Trans. Microwave Theory Tech.* (*Special Issue on Biological Effects of Microwaves*), vol. MTT-19, pp. 187–196, Feb. 1971.

[5] H. N. Kritikos and H. P. Schwan, "Hot spots generated in conducting spheres by electromagnetic waves and biological implications," *IEEE Trans. Bio-Med. Eng.*, vol. BME-19, pp. 53–58, Jan. 1972.

[6] W. T. Joines and R. J. Spiegel, "Resonance absorption of microwaves by the human skull," *IEEE Trans. Bio-Med. Eng.* (Commun.), vol. BME-21, pp. 46–48, Jan. 1974.

[7] C. M. Weil, "Absorption characteristics of multi-layered sphere models exposed to UHF microwave radiation," in *1974 IEEE S-MTT Int. Symp.*, (Atlanta, Georgia, June 1974), pp. 109–111.

[8] J. C. Lin, A. W. Guy, and C. C. Johnson, "Power deposition in a spherical model of man exposed to 1–20-MHz electromagnetic fields," *IEEE Trans. Microwave Theory Tech. 1973 Symp. Issue*, vol. MTT-21, pp. 791–797, Dec. 1973.

[9] C. H. Durney, C. C. Johnson, and H. Massoudi, "Long-wavelength analysis of plane wave irradiation of a prolate spheroid model of man," *IEEE Trans. Microwave Theory Tech.*, vol. MTT-23, pp. 246–253, Feb. 1975.

[10] D. R. Justesen and N. W. King, in *1970 Symp. Proc. Biological Effects and Health Implications Microwave Radiation*, U. S. Pub. Health Serv., BRH/DBE 70-2, 1970, pp. 154–179.

[11] D. R. Justesen, D. M. Levinson, R. L. Clarke, and N. W. King, *J. Microwave Power*, vol. 6, pp. 237–258, 1971.

[12] H. S. Ho, E. I. Ginns, and C. L. Cristman, "Environmentally controlled waveguide irradiation facility," *IEEE Trans. Microwave Theory Tech.* (Short Papers), vol. MTT-21, pp. 837–840, Dec. 1973.

[13] R. D. Phillips, E. L. Hunt, and N. W. King, "Field measurements, absorbed dose, and biological dosimetry of microwaves," presented at the N. Y. Acad. Sci. Conf. Biological Effects of Nonionizing Radiation, New York, Feb. 1974.

[14] A. W. Guy and S. Korbel, "Dosimetry studies on a UHF cavity exposure chamber for rodents," in *Summary of Presented Papers, Microwave Power Symp.* (Ottawa, Ont., Canada May 1972), pp. 180–193.

[15] S. J. Allen, "Measurements of power absorption by human phantoms immersed in radio frequency fields," N. Y. Acad. Sci. Conf. Biological Effects of Nonionizing Radiation, New York, Feb. 1974.

[16] J. Van Bladel, *Electromagnetic Fields*. New York: McGraw-Hill, 1964.

[17] H. P. Schwan, "Electrical properties of tissues and cells," *Advan. Biol. Med. Phys.*, vol. 5, pp. 147–209, 1957.

[18] A. W. Guy, Dep. Rehabilitation Medicine, Univ. Washington, Seattle, private communication.